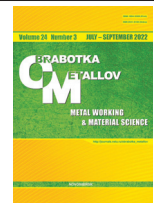




## Obrabotka metallov -

## Metal Working and Material Science

Journal homepage: [http://journals.nstu.ru/obrabotka\\_metallov](http://journals.nstu.ru/obrabotka_metallov)



### Microstructure and residual stresses of ZrN/CrN multilayer coatings formed by the plasma-assisted vacuum-arc method

Andrey Vorontsov<sup>1, a</sup>, Andrey Filippov<sup>1, b, \*</sup>, Nikolay Shamarin<sup>1, c</sup>, Evgenij Moskvichev<sup>1, d</sup>, Ol'ga Novitskaya<sup>1, e</sup>, Evgenii Knyazhev<sup>1, f</sup>, Yuliya Denisova<sup>2, g</sup>, Andrei Leonov<sup>2, h</sup>, Vladimir Denisov<sup>2, i</sup>

<sup>1</sup> Institute of Strength Physics and Materials Sciences SB RAS, 2/4 per. Academicheskii, Tomsk, 634055, Russian Federation

<sup>2</sup> Institute of High Current Electronics SB RAS, 2/3 per. Academicheskii, Tomsk, 634055, Russian Federation

<sup>a</sup>  <https://orcid.org/0000-0002-4334-7616>,  [vav@ispms.ru](mailto:vav@ispms.ru), <sup>b</sup>  <https://orcid.org/0000-0003-0487-8382>,  [andrey.v.filippov@yandex.ru](mailto:andrey.v.filippov@yandex.ru),  
<sup>c</sup>  <https://orcid.org/0000-0002-4649-6465>,  [shnn@ispms.ru](mailto:shnn@ispms.ru), <sup>d</sup>  <https://orcid.org/0000-0002-9139-0846>,  [em\\_tsu@mail.ru](mailto:em_tsu@mail.ru),  
<sup>e</sup>  <https://orcid.org/0000-0003-1043-4489>,  [nos@ispms.tsc.ru](mailto:nos@ispms.tsc.ru), <sup>f</sup>  <https://orcid.org/0000-0002-1984-9720>,  [zhenya4825@gmail.com](mailto:zhenya4825@gmail.com),  
<sup>g</sup>  <https://orcid.org/0000-0002-3069-1434>,  [yukolubaeva@mail.ru](mailto:yukolubaeva@mail.ru), <sup>h</sup>  <https://orcid.org/0000-0001-6645-3879>,  [laa-91@yandex.ru](mailto:laa-91@yandex.ru),  
<sup>i</sup>  <https://orcid.org/0000-0002-5446-2337>,  [volodyadenisov@yandex.ru](mailto:volodyadenisov@yandex.ru)

#### ARTICLE INFO

##### Article history:

Received: 16 May 2022

Revised: 31 May 2022

Accepted: 18 June 2022

Available online: 15 September 2022

##### Keywords:

Coating  
 TEM investigation  
 Nitrides  
 X-Ray analysis  
 Phase composition

##### Funding

The work was carried out with the financial support of the Russian Federation represented by the Ministry of Science and Higher Education (project No. 075-15-2021-1348) within the framework of event No. 1.1.16.

##### Acknowledgements

Research were partially conducted at core facility "Structure, mechanical and physical properties of materials".

#### ABSTRACT

**Introduction.** The current state of the art in the field of hard coatings application requires the formation of nanostructured compositions using different chemical elements. Modern hard coatings are able to combine different properties such as high hardness, wear resistance, corrosion resistance. At present, coatings formed by layer-by-layer deposition of zirconium and chromium nitrides are promising. When depositing combinations of chemical elements on various substrates, studies are required aimed at investigating its microstructure and, mainly, residual stresses formed during the deposition of multilayer coatings. **The purpose of this work** is to investigate the structural-phase state and residual stresses of *ZrN/CrN* system coatings formed by plasma-assisted vacuum-arc method from the gas phase. **Research methods.** Samples with coatings of zirconium and chromium nitrides deposited on substrates of hard alloy *VK8* are investigated. Transmission electron microscopy is used to study the microstructural characteristics of multilayered coatings and X-ray diffraction analysis is used to quantify macroscopic stresses. **Results and discussion.** Based on the experimental results obtained it is found that changing the modes of deposition of multilayer *ZrN/CrN* coatings with regard to rotation speeds of table and substrate holder leads to variations in microstructure, morphology and internal stresses of surface layers of multilayer coatings. It is shown that by changing conditions for the multilayer coating deposition the possibilities of forming *ZrN/CrN* coatings on the substrate made of *VK8* alloy with nanoscale thickness of coating layers open up. X-ray diffraction analysis indicates mainly insignificant stresses, and at high table and substrate rotation speeds – high compressive stresses in the multilayer coating. Transmission electron microscopy revealed that *CrN* and *ZrN* coatings have a common multilayer coating growth texture at low rotation speeds, and at high speeds a textural misorientation of the phases of the coating layers is observed. Based on the results obtained it is possible to recommend coatings of *ZrN/CrN* system as hard coatings.

**For citation:** Vorontsov A.V., Filippov A.V., Shamarin N.N., Moskvichev E.N., Novitskaya O.S., Knyazhev E.O., Denisova Yu.A., Leonov A.A., Denisov V.V. Microstructure and residual stresses of ZrN/CrN multilayer coatings formed by the plasma-assisted vacuum-arc method. *Obrabotka metallov (tehnologiya, oborudovanie, instrumenty) = Metal Working and Material Science*, 2022, vol. 24, no. 3, pp. 76–89. DOI: 10.17212/1994-6309-2022-24.3-76-89. (In Russian).

#### \* Corresponding author

Vorontsov Andrey V., Ph.D. (Engineering), Research assistant  
 Institute of Strength Physics and Materials Sciences SB RAS,  
 2/4 per. Academicheskii,  
 634055, Tomsk, Russian Federation  
 Tel.: 8 (983) 239-34-17, e-mail: vav@ispms.ru

## Introduction

Nitride coatings made of either  $ZrN$  or  $CrN$  possess high mechanical corrosion-resistant and tribological characteristics and therefore are widely used in applications where protection of the base underlying materials against the above mentioned factors is required [1, 2]. In particular, this is especially true for  $CrN$  coatings that begin occupying more and more attention of the researchers [3, 4]. Chromium nitride coatings can be obtained using either vapor deposition or arc-ion plating [2].

Zirconium nitride coatings can be used in aero-space applications as thermal or erosion barriers as well as for extending the service life of the metal cutting tools [5]. Cathodic arc  $ZrN$  coatings may be used for protection of radioactive waste storage tanks against corrosion [6].

The research literature search shows that there are multilayer coatings containing combinations of alternating metallic, ceramic and amorphous layers. Such an approach allows combining various strength and functional characteristics of the constituent layers for achieving improved synergistic performance of the entire coating. For instance, addition of a  $CrN$  layer when preparing the multilayer  $AlTiN/CrN/ZrN$  coatings allowed reducing the residual stresses depending on the  $CrN$  layer thickness [7]. Vapor deposition of nanosize thickness  $CrN/ZrN$  and  $CrN/CrAlN$  layers on stainless steel substrates was carried out to improve the corrosion resistance of the fuel proton exchange membrane cells [8]. It was found that corrosion resistance of  $CrN/ZrN$  multilayer coatings proved to be much higher than that of less chemically stable  $CrN/CrAlN$  ones.

Vacuum-arc deposited  $ZrN/CrN$  multilayer coatings with  $ZrN/CrN$  bi-layer of different thickness were prepared [9] to show that the thickness reduction allowed increasing the coating hardness while maintaining acceptable the other mechanical characteristics. In addition, the effect of nitrogen atomic concentration on the microhardness and microstructure characteristics of the multilayer coatings was revealed. Summarizing the information reported in the relevant literatures sources it could be stated that the multilayer nitride coatings allow improving mechanical, anti-corrosion and anti-wear characteristics of the substrates [8, 10–15]. Such a conclusion allowed us to suggest that deposition of multilayer  $ZrN/CrN$  coatings on the  $WC-8\text{ wt.\%Co}$  cermet has potential for improving the tribological and anti-wear characteristics of the metal processing tools.

The objective of this work can be formulated as follows: study texturing and residual macrostresses in the of multilayer plasma-assisted vacuum-arc deposited  $ZrN/CrN$  coatings as well as evaluate the applicability of the deposition method inviting both earlier obtained [16] and below disclosed results.

## Methods and materials

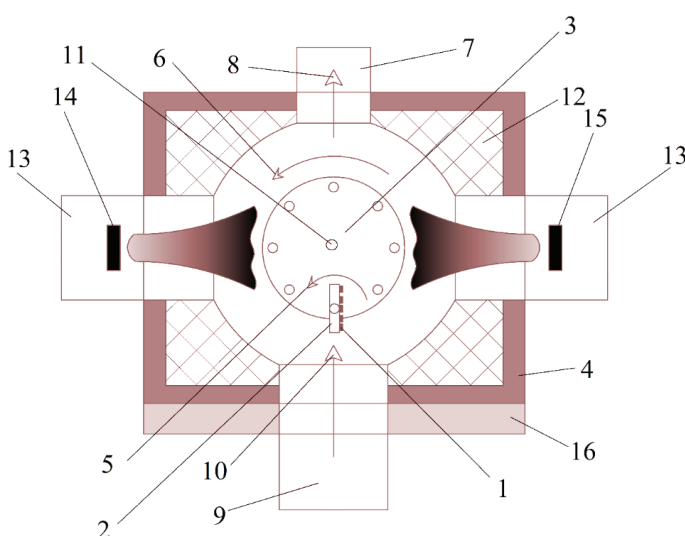


Fig. 1. Scheme of the plant for a  $ZrN/CrN$  multilayer nanostructured coating deposition

A scheme of the plasma-assisted vacuum-arc deposition shows the  $WC-8\text{ wt.\%Co}$  substrate (Fig. 1, pos. 1) mounted successively on the sample holder (Fig. 1, pos. 2) and table (Fig. 1, pos. 3) inside the vacuum chamber (Fig. 1, pos. 4). Sample holder and table were independently rotated during the deposition as shown by corresponding arrows (Fig. 1, pos. 5) and (Fig. 1, pos. 6), respectively. Such a planetary rotation of the sample was chosen to adapt the deposition of multilayer coatings so that the total sample's rotation rate was directly proportional to that of the table.

The internal vacuum chamber volume was evacuated using a turbomolecular pump (Fig. 1, pos. 7) as shown by the arrow (Fig. 1, pos. 8). An inert gas was then supplied via a plasma torch

(Fig. 1, pos. 9) as shown by arrow (Fig. 1, pos. 10) to provide the residual working pressure. On filling the chamber, a gas discharge was ignited at 40 A and bias voltage 700 V with simultaneous preheating the sample to 400°C. The sample's temperature was controlled using a thermocouple (Fig. 1, pos. 11). A thermal shield (Fig. 1, pos. 12) was mounted to avoid the excess heating of the chamber elements.

Ion bombardment cleaning and chemical activation of the sample's surface was carried out and then an argon and nitrogen (90/10) gas mixture was supplied into the chamber up to reaching the working pressure level. Next step was igniting the 80 A arc discharges on both evaporators (Fig. 1, pos. 13). Each of the evaporators contained a single cathode made of the deposited material (Fig. 1, pos. 14 and 15), i.e. either 99.5% purity Zr or 99.9 % purity Cr.

A chamber door (Fig. 1, pos. 16) served for extracting the sample holder and samples after finishing the deposition.

The table rotation rate was varied during the deposition as follows: 0.5 RPM, 3.5 RPM and 8.0 RPM for samples *ZrN/CrN-0.5*, *ZrN/CrN-3.5* and *ZrN/CrN-8*, respectively. The resulting sample's holder rotation rates were then as follows: 20; 140; 320 RPM.

The deposited layers were characterized using *TEM* and synchrotron *XRD* (Synchrotron Source VEPP-3). *TEM* allowed characterizing phases formed and inter-layer boundary misorientation. The *XRD* allowed obtaining the residual stress magnitudes and nitride phase contents.

The synchrotron radiation with wavelength 1.540598 Å was used for performing quantitative  $\sin^2\Psi$ -method analysis of residual stresses formed in the multilayer coatings during deposition and cooling. The required for the analysis data on elasticity modulus were obtained from nanoindentation experiments on these multilayer *ZrN/CrN-0.5*, *ZrN/CrN-3.5* and *ZrN/CrN-8* coatings and were at the level of 364, 359 and 436 GPa, respectively [16]. The Poisson ratio values for *ZrN* and *CrN* were assumed as 0.24 and 0.28, respectively [17, 18].

## Results and discussion

*TEM* studies allowed revealing both morphological and orientation differences among the multilayer coatings as depended on the sample's planetary rotation rates. Fig. 2 shows the bright-field *TEM* images of the *ZrN/CrN-0.5*, *ZrN/CrN-3.5* and *ZrN/CrN-8* multilayer coatings obtained at different rotation rates of the holder. All *ZrN/CrN* coatings are composed of alternating nitride layers but at least two different layer types can be observed in the *ZrN/CrN-0.5* coating. The first one shows formation of nanoscale thickness layers the same as those in the *ZrN/CrN-3.5* and *ZrN/CrN-8* coatings. The nanoscale layer thicknesses are shown in the *TEM* images as denoted by the "h" letter). Accelerating both table and holder rotation rate resulted in reducing the nitride layer thicknesses (Fig. 2 d) and it could be suggested from the plot that there is a linear dependence between the holder rotation rate and layer thickness. A regression equation was reconstructed to describe such a dependence that allowed observing the layer thickness tended to zero if the rotation rate approached to the ordinate axis at  $592\pm 58$  RPM where both nitrides would be homogeneously distributed across the coating. In such a situation it would be plausible formation of either mixed *ZrCrN* nitride or amorphous layer as discussed below.

The second type of layers are submicron thickness ones that are formed at low rate rotations of both table and holder (Fig. 2, a). These submicron layers are composed of the alternating nitride nanoscale ones. The *EDS* element profiles were obtained on the *ZrN/CrN-0.5* coating deposited at the holder rotation rates of 20 RPM (Fig. 3, a). Periodic element concentration dependencies along the line in Fig. 3 a allow suggesting that these submicron layers are of  $120\pm 8$  nm mean thickness.

*SAED* analysis of phases formed in the coatings showed the presence of both nitrides (Fig. 3). However, there are some specific features as those identified from the bright field images (see circles in Fig. 2, a-c). First of all, this relates to crystallite orientations in the layers. Samples of *ZrN/CrN-0.5* and *ZrN/CrN-3.5* were characterized by the presence of an [111] axis zone common for the *ZrN* and *CrN SAED* patterns (Fig. 3 a, b). On the contrary, the *SAED* pattern from *ZrN/CrN-8* sample exposes a common *ZrN/CrN* axis zone [0-11] as well as extra *SAED* pattern from the *ZrN* with different axis zone [1-21]. In other words, there is

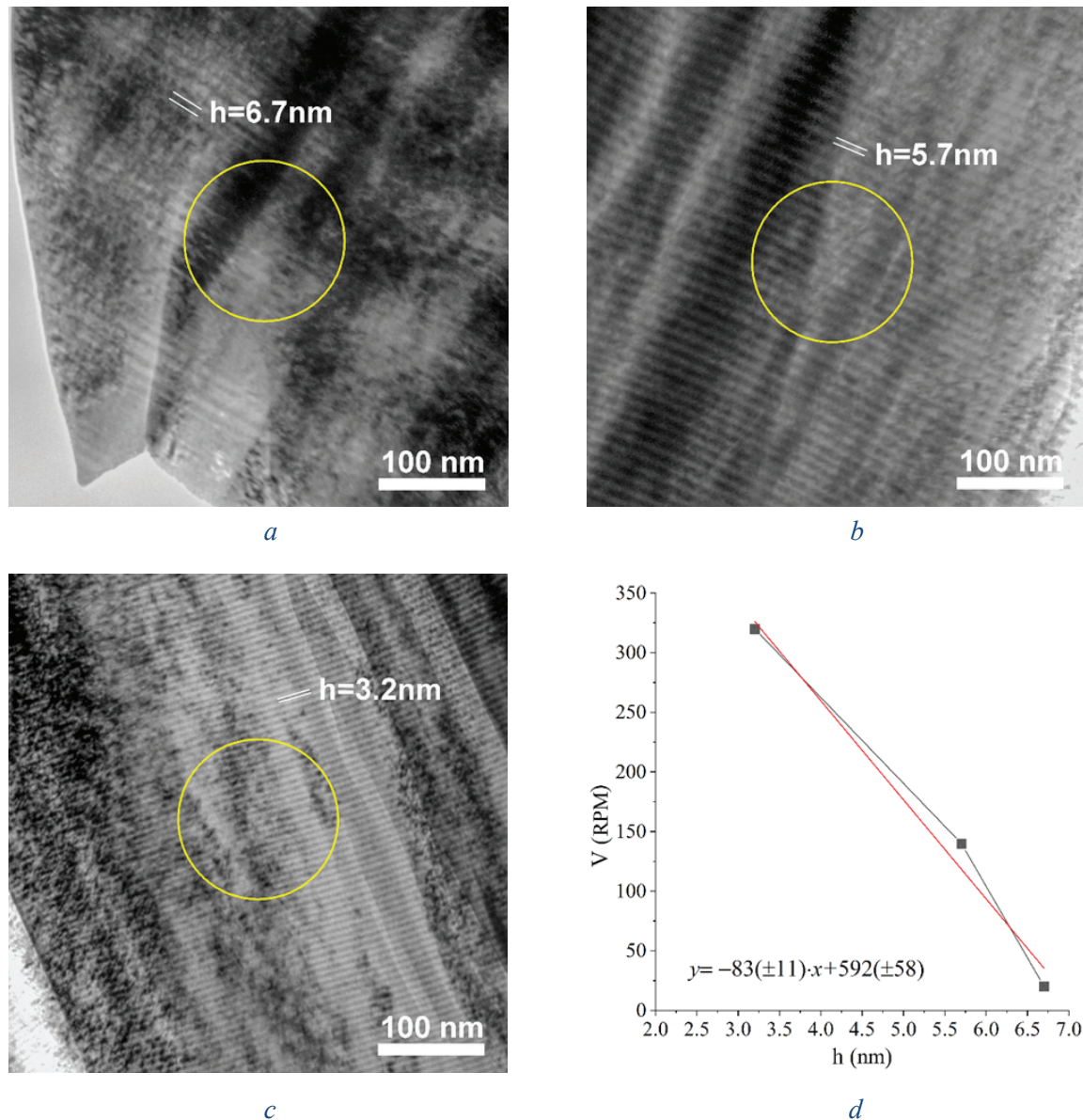


Fig. 2. Bright field image of multilayer coating formed at  $ZrN/CrN-0.5$  (a),  $ZrN/CrN-3.5$  (b),  $ZrN/CrN-8$  (c) and linear approximation of the table and substrate holder rotation speeds as a function of the thickness of nanometer coating layers (d)

preferential orientation relationship between  $ZrN$  and  $CrN$  during deposition at low rotation rates while it is violated at higher rotation rates with the common zone axis rotation and partial misorientation of the  $ZrN$ .

Azimuthal  $ZrN/CrN$  layer misorientation is higher in samples  $ZrN/CrN-0.5$  and  $ZrN/CrN-3.5$ , deposited at low rotation rates. For comparison, the azimuthal misorientation in these samples was about  $18^\circ$  as compared to  $6^\circ$  in the  $ZrN/CrN-8$  (Fig. 3, b–d).

Therefore, sample rotation during deposition has some effect on the coating microstructure, in particular, the orientation relationship between the layers. Such an effect may be the reason behind the residual stresses formed in the coatings during cooling. Residual stress level is one of the most important characteristics that determine mechanical and functional characteristics of the multilayer coatings. Therefore, the research can not be limited only by studying the microstructures only.

Residual stress levels were studied using the well-known  $\sin^2\Psi$ -method but with utilizing the synchrotron X-ray radiation. Quantitative stress level can be estimated using expression 1 as follows [19]:

$$\sigma_x = -\frac{E}{2(1 + \nu_{MII})} \text{ctg}\Theta_0 \frac{\partial(2\Theta_{\Psi_x})}{\partial(\sin^2 \Psi)} \frac{\pi}{180} \quad [\text{MPa}], \quad (1)$$

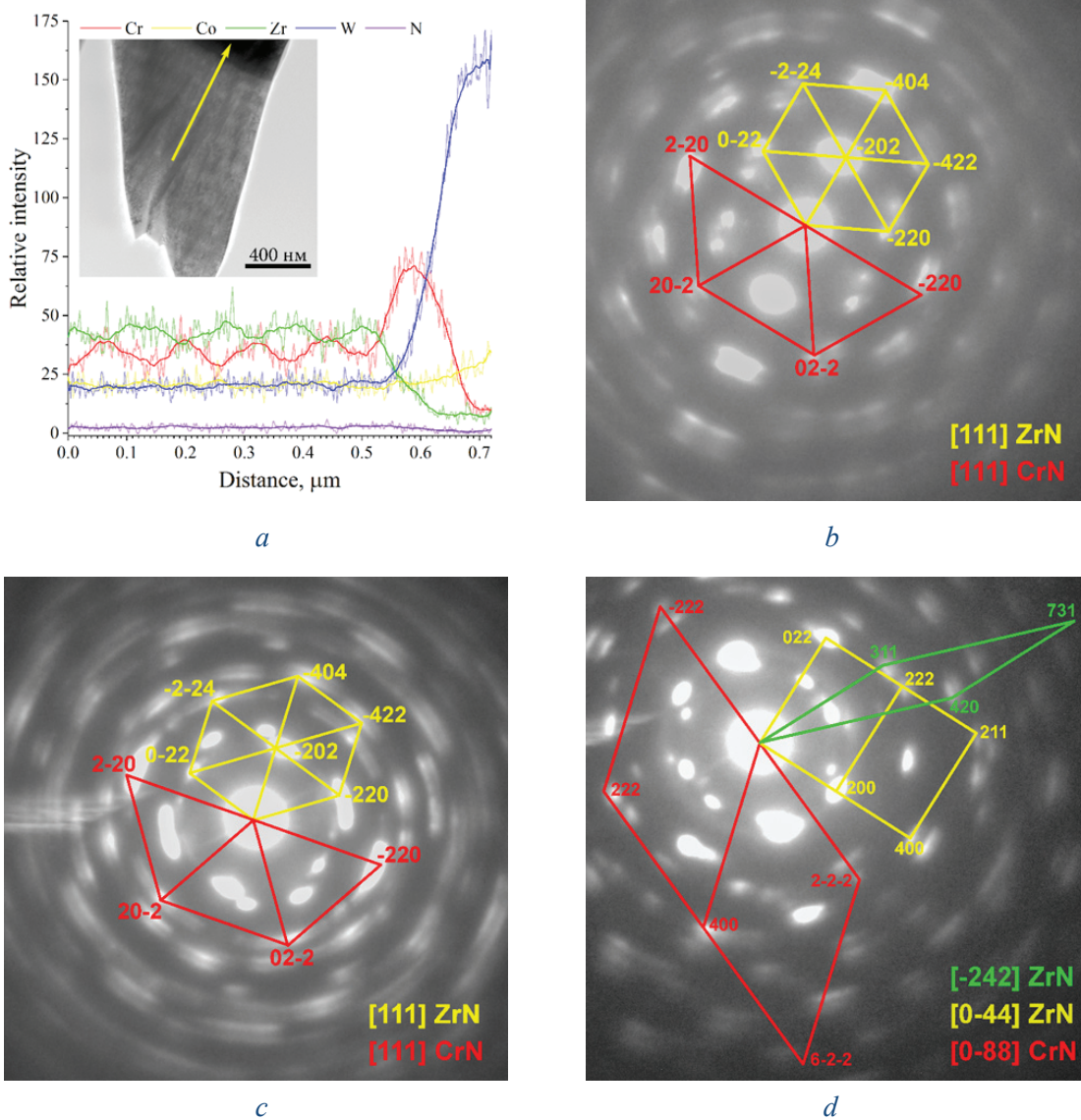


Fig. 3. Chemical element distribution in  $ZrN/CrN-0.5$  multilayer coating (a), micro diffraction patterns of multilayer coatings formed at  $ZrN/CrN-0.5$  (b),  $ZrN/CrN-3.5$  (c) and  $ZrN/CrN-8$  (d) modes

where  $E$  is the effective elasticity modulus obtained from nanoindentation;  $\nu_{ML}$  is the *Poisson* ratio,  $\Theta_0$  is the diffraction angle of incident synchrotron beam on a stress-free coating;  $\Theta_{\Psi_x}$  is the diffraction angle of incident synchrotron beam on a coating with residual stress for crystalline planes normal to ( $\Psi$ ) the incident beam axis.

The first stage was obtaining primary *Bragg-Brentano* diffraction patterns and  $2\Theta_0$  reflection positions from the  $ZrN/CrN$  multilayer coatings according to symmetrical *XRD* procedure (Fig. 4). *XRD FCC* peaks such as  $(200)_{CrN}$  and  $(222)_{ZrN}$  were chosen for determining the residual stress taking into account the best accuracy reasons. An obstacle was that there were *WC* peaks shining from underneath substrate in the form of very narrow peaks.

The *XRD* pattern in Fig. 4 allows observing some variation of a textured coating's component. Thus, almost invisible at  $2\Theta=56.7^\circ$   $(220)_{ZrN}$  peak in the  $ZrN/CrN-0.5$  coating became very noticeable in samples  $ZrN/CrN-3.5$  and  $ZrN/CrN-8$ , i.e at higher rotation rates. Such a finding allows suggesting that the  $ZrN$  crystallites have no preferential growth axis during deposition at faster rotation.

Asymmetrical *XRD* were then carried out at  $\Psi$  angles  $0^\circ, 5^\circ, 10^\circ, 15^\circ, 20^\circ, 25^\circ, 30^\circ$  and a series of corresponding diffraction patterns in the vicinity of the  $(222)_{ZrN}$  peak (red line) are shown in Fig. 5 for sample  $ZrN/CrN-0.5$ .

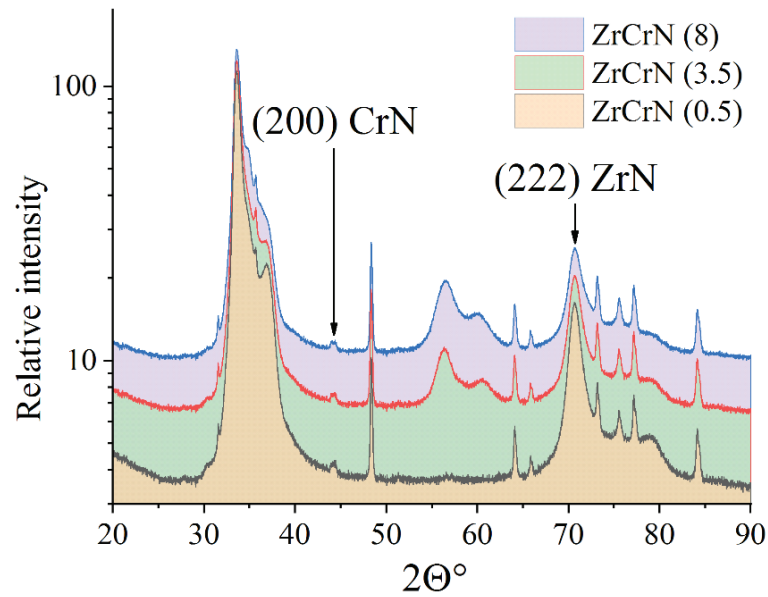


Fig. 4. X-ray diagrams of the formed *ZrN/CrN* multilayer coated samples obtained by symmetrical imaging (*Bragg-Brentano* focusing) with marking of peaks subjected to further series of asymmetrical imaging to determine stresses by  $\sin^2\Psi$  method

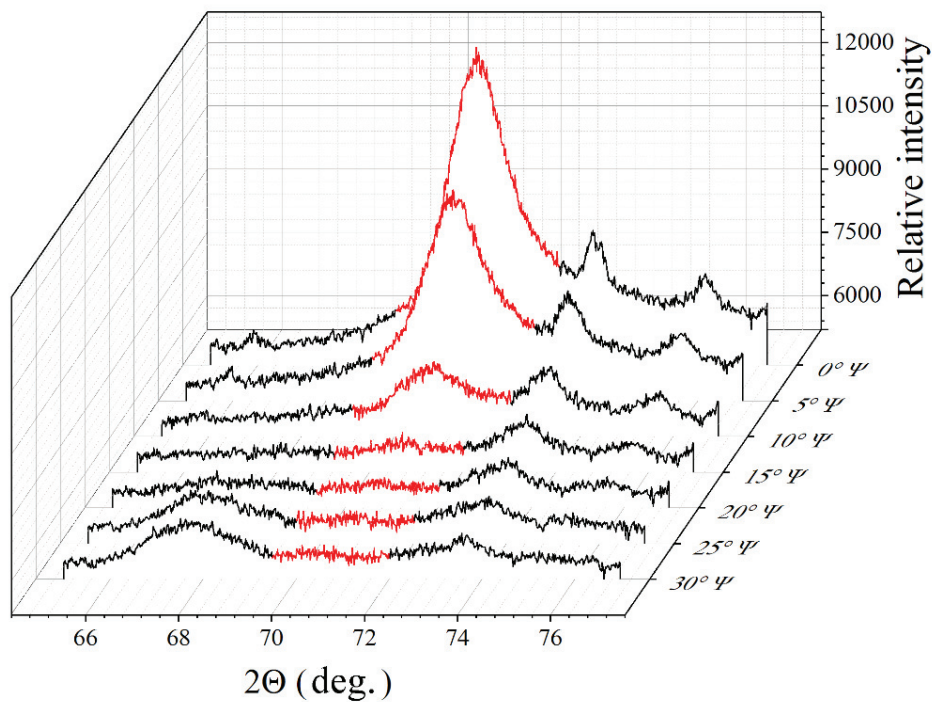


Fig. 5. Series of asymmetric synchrotron radiation surveys in the range of  $2\Theta$   $65^\circ - 77^\circ$  for the *ZrN* phase peak (222) of sample *ZrN/CrN-0.5* with a variation of angle  $\Psi$  from  $0^\circ$  to  $30^\circ$  with a step of  $5^\circ$ . The angular range of the analyzed peak is highlighted in red

When the angle position of the *XRD* peaks was accurately determined, the data were represented in the  $2\Theta_{\Psi_x}$ - $\sin^2\Psi$  domain and then linearly approximated (Fig. 6).

The residual stress levels  $\sigma_x$  can be obtained using equation 2:

$$\sigma_x = MK[\text{MPa}], \quad (2)$$

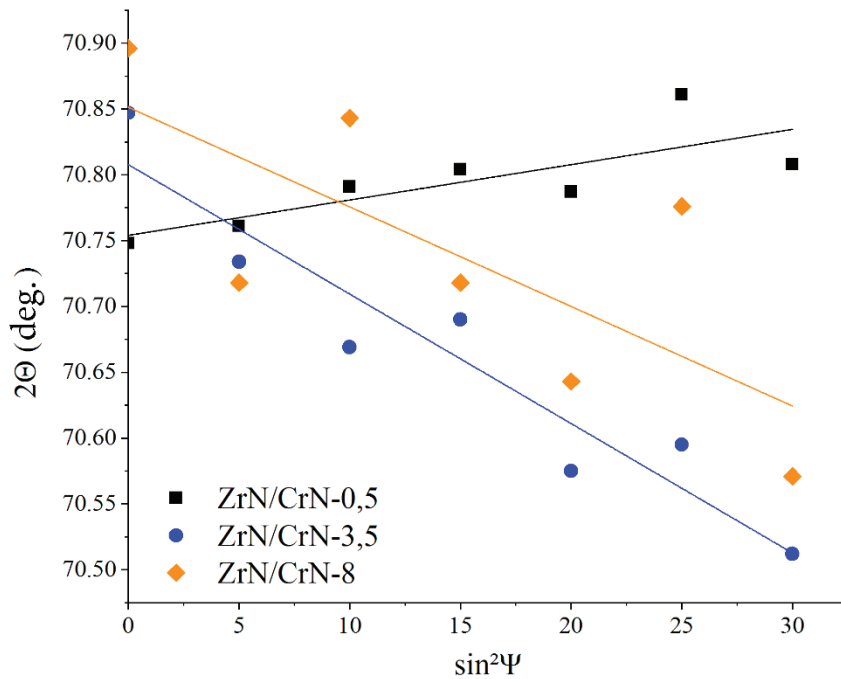


Fig. 6. Linear dependence of diffraction maximum position (222) of *ZrN* phase on  $\sin^2\Psi$  for samples of multilayer coatings deposited at different rotational speeds of table and substrate holder

where

$$M = -\frac{E}{2(1 + \nu_{MII})} \text{ctg}\Theta_0 \frac{\pi}{180}, \text{ MPa/grad}, \tag{3}$$

$$K_{\Delta} = \frac{\partial(2\Theta_{\Psi_x})}{\partial(\sin^2 \Psi)}, \text{ grad} \tag{4}$$

Consequently, quantitative determination of the residual stress in the multilayer coatings requires determining angle  $\Theta_0$  of the stress-free material from the  $2\Theta_{\Psi_x} - \sin^2\Psi$  plot, where  $2\Theta_0$  is the extrapolation of linear approximation  $2\Theta_{\Psi_x} - \sin^2\Psi$  [20]. Coefficient  $K_{\Delta}$  is determined from the  $2\Theta_{\Psi_x} - \sin^2\Psi$  approximation line slope as shown by equation 4.

Stress coefficient  $M$  was calculated according to equation 3 using the earlier obtained values of  $\nu_{ML}$ ,  $E$ ,  $\Theta_0$ . The residual stress magnitudes in the multilayer coatings were obtained using equation 2 (see Table 1).

Similar to the previous stages, the residual stress magnitudes were obtained from *XRD* patterns in the vicinity of  $(200)_{CrN}$  angle position at  $2\Theta = 44^\circ$  (Fig. 7).

Angle positions of the  $(200)_{CrN}$  are represented in the  $2\Theta_{\Psi_x} - \sin^2\Psi$  domain in Fig. 8.

Finally, some data as well as residual stress magnitudes were shown in Table 2.

Table 1

Calculated values for determining the residual stresses and the result of calculating the residual stresses in the plane of the surface of the multilayer coating samples for the *ZrN* phase

Coating	$2\Theta_0, ^\circ$	Coefficient $M$ , MPa/grad	Coefficient $K$ , grad	Residual stress, MPa
ZrN/CrN-0.5	$70.754 \pm 0.017$	$-2.393 \times 10^3$	$0.003 \pm 0.001$	-6.437
ZrN/CrN-3.5	$70.808 \pm 0.026$	$-2.235 \times 10^3$	$-0.010 \pm 0.001$	22.000
ZrN/CrN-8	$70.851 \pm 0.057$	$-2.599 \times 10^3$	$-0.008 \pm 0.003$	19.65

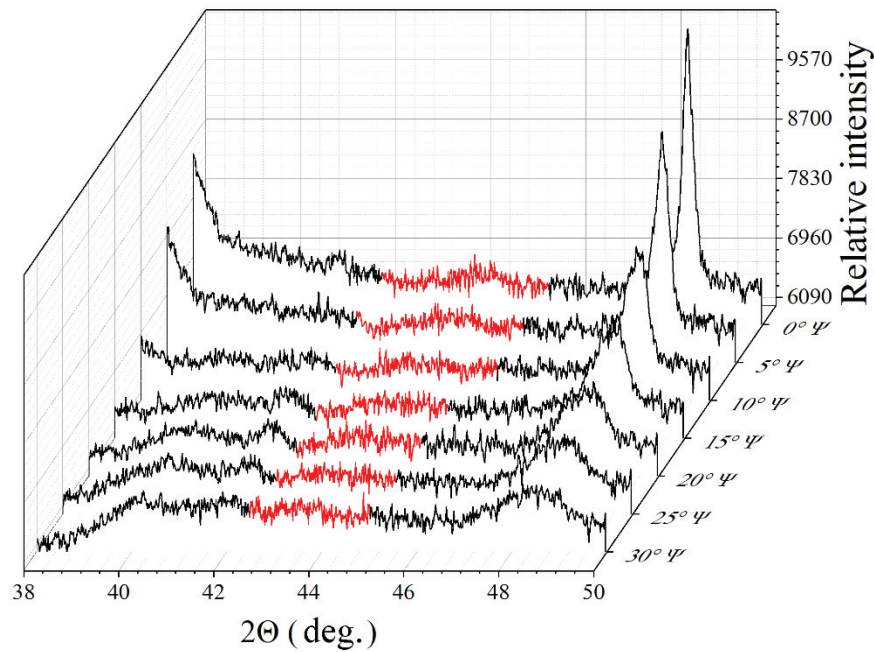


Fig. 7. Series of asymmetric surveys using synchrotron radiation in the range of angle  $2\theta$   $38^\circ - 50^\circ$  for the peak (200) of the  $CrN$  phase with a variation of angle  $\Psi$  from  $0^\circ$  to  $30^\circ$  with a step of  $5^\circ$

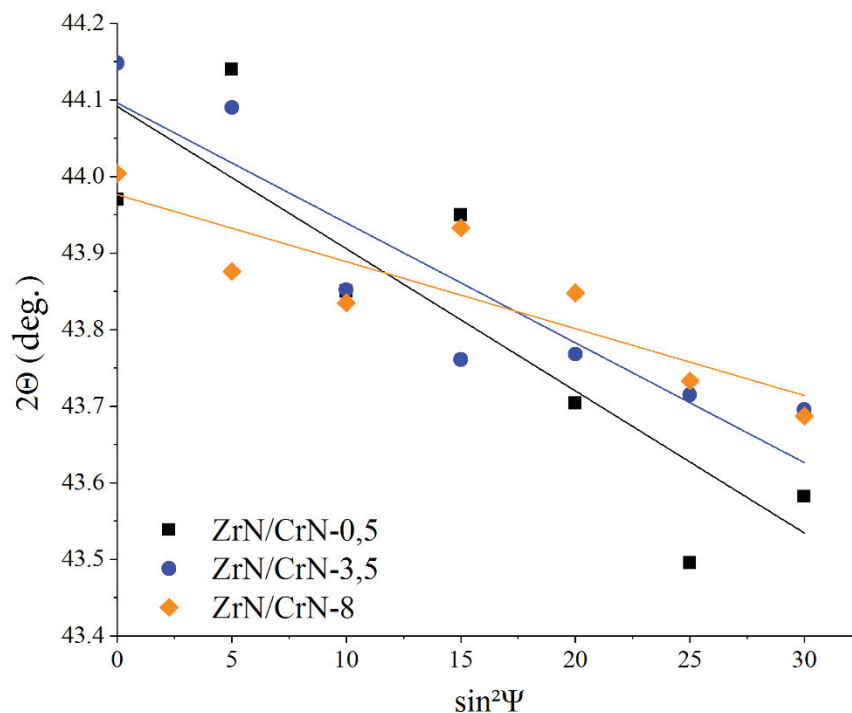


Fig. 8. Linear dependence of diffraction maximum position (200) of  $CrN$  phase on  $\sin^2\Psi$  for multilayer coating samples deposited at different table and substrate rotation speeds

The asymmetrical  $XRD$  patterns in Fig. 4 and 6 are shown as the examples that allow identifying the fact that residual stresses were rather low for all the coatings obtained using the plasma-assisted vacuum-arc method. These stresses are either tensile or compressive as in case of  $CrN$  in the  $ZrN/CrN-8$  coating (Table 2).

**Results of quantitative determination of stress values in in the plane of the surface of the multilayer coating samples for the CrN phase during synchrotron studies**

Coating	$2\Theta_0, ^\circ$	Coefficient M, MPa/grad	Coefficient, K, grad	Residual stress, MPa
ZrN/CrN-0.5	$44.092 \pm 0.084$	$-4.520 \times 10^3$	$-0.019 \pm 0.005$	839
ZrN/CrN-3.5	$44.096 \pm 0.053$	$-4.301 \times 10^3$	$-0.016 \pm 0.003$	674
ZrN/CrN-8	$43.976 \pm 0.041$	$9.441 \times 10^5$	$-0.009 \pm 0.002$	-8,251

Taking into account the results of *TEM* one may conclude that increasing the rotation rates of table and holder is accompanied by misorientation and reorientation of the nitride layers, increasing its hardness and elasticity modulus [16] and transition from tensile to compressive residual stress. Despite microstructural characteristics of the coatings, specifics of texturing and residual stress indicate on the positive effect of increasing the rotation rate during the multilayer coating deposition, there are some aspects to be studied to determine the applicability of such a technique as well as its effect on the functional characteristics of the coatings.

### Conclusions

Plasma-assisted vacuum-arc *ZrN/CrN* multilayer coatings were investigated for microstructure, hardness and residual stress. As shown, the rotation rates of both table and sample's holder have its effect on the above noted characteristics.

*ZrN* and *CrN* crystallites grow along the common axis with the interlayer misorientation about  $18^\circ$  at low rotation rates. Increasing the rotation rate resulted in breaking the orientation relationship with increased misorientation between the *ZrN* crystallites.

The thickness of the alternating *ZrN* and *CrN* layers is almost linearly reduced when increasing the substrate rotation rate.

The *XRD* shows that residual tensile stress in the *ZrN/CrN-0.5* and *ZrN/CrN-3.5* multilayer coatings are low whereas it becomes compressive in the fast rotated *ZrN/CrN-8*.

### References

- Berrios-Ortiz J.A., La Barbera-Sosa J.G., Teer D.G., Puchi-Cabrera E.S. Fatigue properties of a 316L stainless steel coated with different ZrN deposits. *Surface and Coatings Technology*, 2004, vol. 179, pp. 145–157. DOI: 10.1016/S0257-8972(03)00808-9.
- Zhang M., Li M.K., Kim K.H., Pan F. Structural and mechanical properties of compositionally gradient CrNx coatings prepared by arc ion plating. *Applied Surface Science*, 2009, vol. 255, pp. 9200–9205. DOI: 10.1016/J.APSUSC.2009.07.002.
- Zhang M., Lin G., Lu G., Dong C., Kim K.H. High-temperature oxidation resistant (Cr, Al)N films synthesized using pulsed bias arc ion plating. *Applied Surface Science*, 2008, vol. 254, pp. 7149–7154. DOI: 10.1016/J.APSUSC.2008.05.293.
- Liu C., Bi Q., Ziegele H., Leyland A., Matthews A. Structure and corrosion properties of PVD Cr–N coatings. *Journal of Vacuum Science and Technology A: Vacuum, Surfaces, and Films*, 2002, vol. 20, pp. 772–780. DOI: 10.1116/1.1468651.
- Mernagh V.A., Kelly T.C., Ahern M., Kennedy A.D., Adriaansen A.P.M., Ramaekers P.P.J., McDonnell L., Koekoek R. Adhesion improvements in silicon carbide deposited by plasma enhanced chemical vapour deposition. *Metallurgical Coatings and Thin Films*, 1991, vol. 1, pp. 462–467. DOI: 10.1016/B978-0-444-89455-7.50087-3.
- Gruss K.A., Zheleva T., Davis R.F., Watkins T.R. Characterization of zirconium nitride coatings deposited by cathodic arc sputtering. *Surface and Coatings Technology*, 1998, vol. 107, pp. 115–124. DOI: 10.1016/S0257-8972(98)00584-2.

7. Chang Y.Y., Chang B.Y., Chen C.S. Effect of CrN addition on the mechanical and tribological performances of multilayered AlTiN/CrN/ZrN hard coatings. *Surface and Coatings Technology*, 2022, vol. 433, pp. 128107. DOI: 10.1016/J.SURFCOAT.2022.128107.
8. Rajabi T., Atapour M., Elmkhah H., Nahvi S.M. Nanometric CrN/CrAlN and CrN/ZrN multilayer physical vapor deposited coatings on 316L stainless steel as bipolar plate for proton exchange membrane fuel cells. *Thin Solid Films*, 2022, vol. 753, p. 139288. DOI: 10.1016/J.TSF.2022.139288.
9. Maksakova O., Simoões S., Pogrebnyak A., Bondar O., Kravchenko Y., Beresnev V., Erdybaeva N. The influence of deposition conditions and bilayer thickness on physical-mechanical properties of CA-PVD multilayer ZrN/CrN coatings. *Materials Characterization*, 2018, vol. 140, pp. 189–196. DOI: 10.1016/J.MATCHAR.2018.03.048.
10. Zhang J.J., Wang M.X., Yang J., Liu Q.X., Li D.J. Enhancing mechanical and tribological performance of multilayered CrN/ZrN coatings. *Surface and Coatings Technology*, 2007, vol. 201, pp. 5186–5189. DOI: 10.1016/J.SURFCOAT.2006.07.093.
11. Huang S.H., Chen S.F., Kuo Y.C., Wang C.J., Lee J.W., Chan Y.C., Chen H.W., Duh J.G., Hsieh T.E. Mechanical and tribological properties evaluation of cathodic arc deposited CrN/ZrN multilayer coatings. *Surface and Coatings Technology*, 2011, vol. 206, iss. 7, pp. 1744–1752. DOI: 10.1016/j.surfcoat.2011.10.029.
12. Zhang Z.G., Rapaud O., Allain N., Merce D., Baraket M., Dong C., Coddet C. Microstructures and tribological properties of CrN/ZrN nanoscale multilayer coatings. *Applied Surface Science*, 2009, vol. 255, iss. 7, pp. 4020–4026. DOI: 10.1016/j.apsusc.2008.10.075.
13. J.A., Souza R.M., De Lima N.B., Tschiptschin A.P. Thick CrN/NbN multilayer coating deposited by cathodic arc technique. *Materials Research*, 2017, vol. 20, pp. 200–209. DOI: 10.1590/1980-5373-MR-2016-0293.
14. Barshilia H.C., Selvakumar N., Deepthi B., Rajam K.S. A comparative study of reactive direct current magnetron sputtered CrAlN and CrN coatings. *Surface and Coatings Technology*, 2006, vol. 201, pp. 2193–2201. DOI: 10.1016/J.SURFCOAT.2006.03.037.
15. Yi P., Zhu L., Dong C., Xiao K. Corrosion and interfacial contact resistance of 316L stainless steel coated with magnetron sputtered ZrN and TiN in the simulated cathodic environment of a proton-exchange membrane fuel cell. *Surface and Coatings Technology*, 2019, vol. 363, pp. 198–202. DOI: 10.1016/J.SURFCOAT.2019.02.027.
16. Filippov A.V., Shamarin N.N., Moskvichev E.N., Novitskaya O.S., Knyazhev E.O., Denisova Yu.A., Leonov A.A., Denisov V.V. Investigation of the structural-phase state and mechanical properties of ZrCrN coatings obtained by plasma-assisted vacuum arc evaporation. *Obrabotka metallov (tekhnologiya, oborudovanie, instrumenty) = Metal Working and Material Science*, 2022, vol. 24, no. 1, pp. 87–102. DOI: 10.17212/1994-6309-2022-24.1-87-102.
17. Sue J.A., Perry A.J., Vetter J. Young's modulus and stress of CrN deposited by cathodic vacuum arc evaporation. *Surface and Coatings Technology*, 1994, vol. 68–69, pp. 126–130. DOI: 10.1016/0257-8972(94)90149-X.
18. Meenaatci A.T.A., Rajeswarapalanichamy R., Iyakutti K. Pressure induced phase transition of ZrN and HfN: a first principles study. *Journal of Atomic and Molecular Sciences*, 2013, vol. 4, no. 4, pp. 321–335. DOI: 10.4208/jams.121012.012013a.
19. Chimmat M., Srinivasan D. Understanding the Residual Stress in DMLS CoCrMo and SS316L using X-ray diffraction. *Procedia Structural Integrity*, 2019, vol. 14, pp. 746–757. DOI: 10.1016/J.PROSTR.2019.05.093.
20. Gorelik S.S., Rastorguev L.N., Skakov Yu.A. *Rentgenograficheskii i elektronnoopticheskii analiz [X-Ray diffraction and electron-optical analysis]*. 2nd ed. Moscow, Metallurgiya Publ., 1970. 366 p.

## Conflicts of Interest

The authors declare no conflict of interest.

© 2022 The Authors. Published by Novosibirsk State Technical University. This is an open access article under the CC BY license (<http://creativecommons.org/licenses/by/4.0/>).